Available online at www.sciencedirect.com
SCIENCE DIRECT®
International Journal of Heat and Mass Transfer 47 (2004) 1403–1412
International Journal of HEAT and MASS TRANSFER
www.elsevier.com/locate/ijhmt

# Rib-induced secondary flow effects on local circumferential heat transfer distribution inside a circular rib-roughened tube

Robert Kiml *, Adrian Magda, Sadanari Mochizuki, Akira Murata

*Department of Mechanical Systems Engineering, Tokyo University of A&T, Koganei-shi, Nakacho 2-24-16, Tokyo 184-8588, Japan*

Received 7 March 2003

**Abstract**

Angled ribs were employed to induce a secondary flow as well as to cause the flow separation and reattachment. They were mounted on the inner surface of a tube with an angle between the plane of each rib and the mean flow direction of 75°, 60° and 45° for the angled ribs and 90° for the transverse ribs. Heat transfer experiment, flow visualization experiment and numerical simulation were conducted in order to clarify the flow structure and its effects on the circumferential heat transfer distribution. The present study explicitly demonstrates the heat transfer superiority of angled ribs over conventional transverse ribs due to a development of the rib-induced secondary flow in a form of a pair of vortices, which convey the colder and higher momentum fluid from the core region towards the heated wall and augment heat transfer especially at the bottom region of the tube.


*Keywords:* Forced convention; Heat transfer augmentation; Secondary flow; Flow separation; Ribs

## 1. Introduction

Among many heat transfer enhancement methods, ribs are the most widely employed technique to augment the heat transfer performance inside channels or tubes. The mechanism of heat transfer enhancement by the conventional ribs is based on the flow separation and reattachment. This can be well demonstrated by the transverse ribs that induce two-dimensional flow phenomenon. The fluid temperature in the core region is always lower than that near the wall when heat is transferred from the wall to the fluid. Therefore, if the cold and higher momentum fluid in the central core region of the tube is by some means carried to the area near the wall, heat transfer will be enhanced. In other words, if the secondary flow occurs, the thickness of both velocity and thermal boundary layers on the wall where the flow from the tube core region hits will become thinner and the heat transfer in that region will be augmented. There has been no enhancement techniques based on this concept suggested in the past for the straight circular tubes. Conventional roughened surfaces (including ribs) are used to mix fluid only near the heat transfer walls. Wire coils, twisted tapes or corrugated tubes do not serve the purpose described above since they induce axisymmetrical swirls or single vortex.

In the past, many studies focused on the techniques for augmenting heat transfer performance in various heat transfer equipments with circular tubes. For example, a lot of studies investigating heat transfer and friction coefficients have been conducted in finned tubes, sand-grained textures, wire-coil inserted tubes, transverse rib-roughened tubes and shell-and-tube heat exchangers by Webb [1], Nozu and Honda [2], Alam and Ghoshdastidar [3], Brognaux [4] and Marner [5]. However, most of these studies focused on heat transfer augmenting techniques affecting the flow only near the tube surface with a limited influence on the flow in the

* Corresponding author. Tel./fax: +81-42-388-7088.
*E-mail address:* robert@mmlab.mech.tuat.ac.jp (R. Kiml).

0017-9310/$ - see front matter © 2003 Elsevier Ltd. All rights reserved.
doi:10.1016/j.ijheatmasstransfer.2003.09.026

**Nomenclature**

| | | | |
|---|---|---|---|
| $A_h$ | heat transfer surface area [m$^2$] | $Pr$ | Prandtl number of air |
| $c_p$ | specific heat of air [J/kg K] | $Re$ | Reynolds number |
| $d$ | tube inner diameter [m] | $T_b$ | local bulk temperature [K], $(T_{in} + (z/L_m)(T_{out} - T_{in}))$ |
| $e$ | rib height [m] | $T_{in}$ | inlet bulk temperatures [K] |
| $I$ | turbulence intensity | $T_{out}$ | outlet bulk temperatures [K] |
| $k$ | air thermal conductivity [W/m K] | $T_w$ | wall temperature [K] |
| $L_m$ | heater length [m] | $u'$ | local flow velocity [m/s] |
| $\dot{m}$ | air mass flow rate [kg/s] | $u_m$ | mean velocity [m/s] |
| $Nu$ | local Nusselt number | $z$ | distance along the tube axis measured from the inlet of the test section [m] |
| $Nu_m$ | mean circumferential Nusselt number for each line of measurement points over $z/de = 1$–11 | $\alpha$ | local heat transfer coefficient [W/m$^2$ K] |
| $Nu_\infty$ | Nusselt number for fully developed flow in a smooth passage | $v$ | air kinematic viscosity [m$^2$/s] |
| $\dot{q}_w$ | wall heat flux [W/m$^2$] | $\rho$ | air density [kg/m$^3$] |

central core region, where the cold and fresh fluid is located. There were also studies by Sethumadhavan and Raja [6], Chen et al. [7], Kidd [8], Vulchanov et al. [9] and Zimparov et al. [10] examining the spirally corrugated tubes, which are geometrically closer to the present study. The corrugated tubes induce a secondary flow in a form of a single vortex, which is still insufficient in bringing larger volume of the cold fluid from the tube core region to the tube surface. In many cases these studies omitted a close examination of flow field and its influences on the overall and detailed heat transfer distribution.

Two studies by Webb et al. [11] and Webb and Eckert [12] investigated the effects of ribs as flow turbulators inside tubes with repeated rib- roughness (transverse ribs). There have been also studies examining the effects of ribs as secondary flow inducers with the helically rib-roughened tubes Gee and Webb [13] and Liu and Jensen [14]. However, the rib-induced secondary flow structure again induced only a single vortex, similar to that induced by the corrugated tubes.

In the present study two different types of ribs are employed: (a) angled ribs (elliptic rings) and (b) the transverse ribs (circular rings). The former is expected to induce the secondary flow as well as to cause the flow separation and reattachment. The ribs are mounted on the inner surface of a circular tube with an angle between the plane of each rib and the mean flow direction of 75°, 60° and 45° for the angled ribs and 90° for the transverse ribs. The study mainly focuses on detailed examination of the rib-induced flow field by numerical simulation. The obtained results are compared with the results from the flow visualization and heat transfer measurements, which were already published and discussed by Kiml et al. [15], Mochizuki et al. [16] and Kiml et al. [17].

## 2. Experimental apparatus and methods

### 2.1. Heat transfer experiment

The heat transfer experiment was performed using a rib-roughened circular tube with the inner diameter of the tube $d = 31$ mm and ribs attached on the inner wall of the channel, as shown in Fig. 1. The heat transfer test section was made from two Bakelite blocks. The inner surface of the test section was covered with a thin electric conductive plastic film, consisting of 180 μm thick polyethylene (PET) layer and a 20 μm thick conductive layer. Uniform wall heat flux conditions were achieved by passing an electric current through the conductive layer of the film.

The wall surface temperature distribution was measured by means of 350 K-type thermocouples with a diameter of 50 μm. The thermocouples for wall temperature measurement were attached along 10 lines, which were parallel to the tube axis and were evenly distributed circumferentially (see Figs. 1 and 2). The inlet and the bulk mean outlet air temperatures were also measured with two and five K-type thermocouples, respectively. The size of the rib cross-section was 3.1 mm in height and 3.1 mm in width and the axial pitch of the ribs was 31 mm for both angled and transverse ribs. Ribs were made of Bakelite and mounted on the inner surface of the test section. The angle between the plane of each rib and the mean flow direction was 75°, 60° and 45° for the angled ribs and 90° for the transverse ribs. The

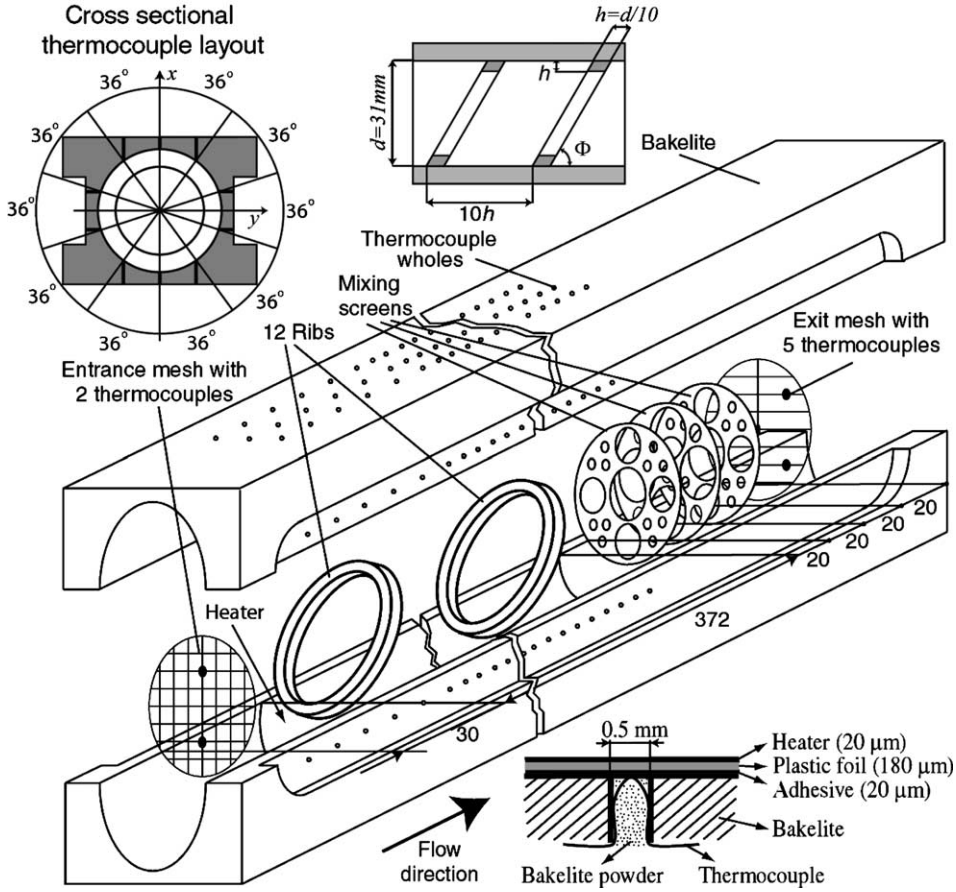


Fig. 1. Schematic of heat transfer test section.

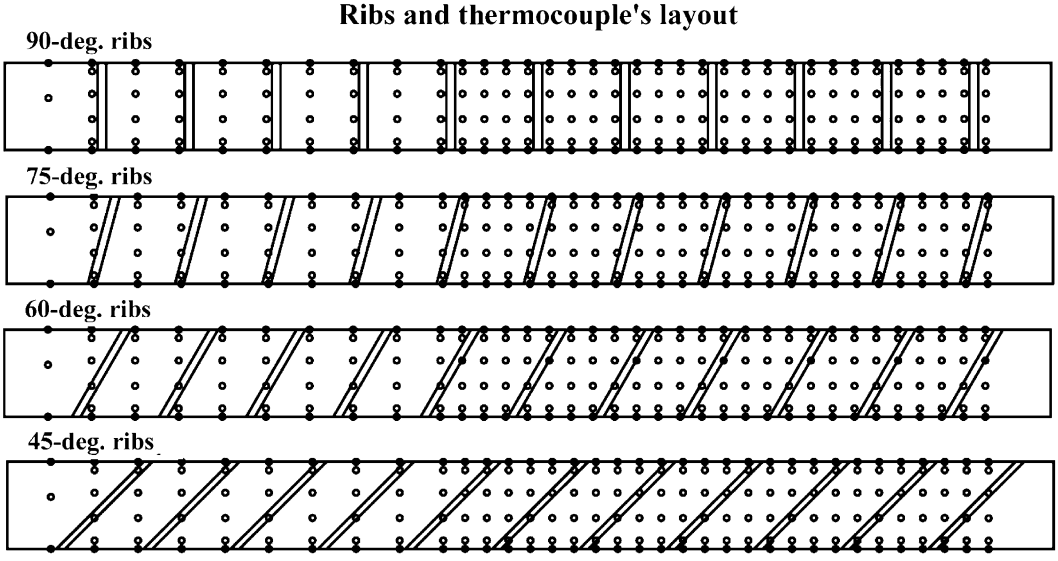


Fig. 2. Thermocouple and rib layout for tubes with 90°, 75°, 60° and 45° ribs.

Reynolds number was varied from $Re = 5000$ to 20,000. For further details please refer to [15,16].

### 2.2. Data reduction for heat transfer experiments

The Reynolds number, wall heat flux, local heat transfer coefficient, friction coefficient and Nusselt numbers in case of the heat transfer experiments were calculated, respectively, as follows:

$$Re = u_m d/v \tag{1}$$

$$\dot{q}_w = \dot{m} c_p (T_{out} - T_{in})/A_h \tag{2}$$

$$\alpha = \dot{q}_w/(T_w - T_b) \tag{3}$$

$$Nu = \alpha d/k \tag{4}$$

$$Nu_\infty = 0.022 Re^{0.8} Pr^{0.5} \tag{5}$$

The mean Nusselt number circumferential distribution over each line of measurement points in the range of $z/d = 1$–11, $Nu_m$, was evaluated as follows:

$$\alpha_{1-11} = \dot{q}_w \Big/ \left[ \int_{z_1}^{z_{11}} (T_w - T_b)\, dz/(z_1 - z_{11}) \right] \tag{6}$$

$$Nu_m = (\alpha_{1-11} d)/k \tag{7}$$

All the physical properties $k$, $v$, $\rho$ and $Pr$ are calculated from the arithmetic mean temperature of the air at the inlet and exit of the test section.

An uncertainty analysis using the ASME Performance Test Codes (ANSI/ASME PTC 19.1-1985), was carried out for the heat transfer experiment. It was estimated that the maximum uncertainty of the Nusselt number within the range of the present experiment was less than 10%.

### 2.3. Flow visualization experiment

Flow visualization using fine plastic-resin particles as tracers was carried out in a circular tube ($d = 100$ mm) made of transparent 5 mm thick Plexiglas. The particles (about 0.2 mm in diameter) were illuminated between the 6th and 8th ribs by an argon laser light-sheet (3 mm thickness) and recorded by a still digital camera and video camera, as shown in Fig. 3. The still camera exposure time was set to 0.5 s to allow the particles to create path lines. Side, Top and Front view flow patterns were taken at many locations to give a clear understanding of the three-dimensional flow structure. All the geometric properties and Reynolds number were the same with those used in the heat transfer experiments. The circumferential locations of the tube surface have been given names "Top" and "Bottom" with respect to the reader's point of view. For further details please refer to [15,16].

### 2.4. Numerical simulation

A numerical study of the flow field in a circular tube with ribs mounted on the inner surface has been performed using the finite volume FLUENT code (commercially available software, version 5.6) with $k$–$\varepsilon$ model of turbulence. The procedure of solving the governing equations of continuity, momentum and energy was pressure-based, whereby the full Navier–Stokes equations were treated in general, body fitted coordinates. Control-volume storage scheme was employed where all variables were stored at the cell center. Second order upwind scheme was used in order to interpolate the face values of computed variables. Implicit segregated solver

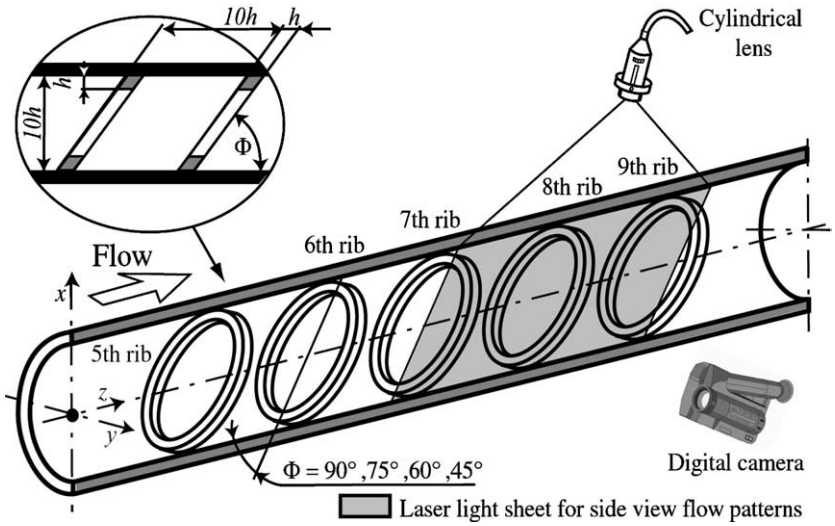


Fig. 3. Schematic of flow visualization performed by particle tracer method.

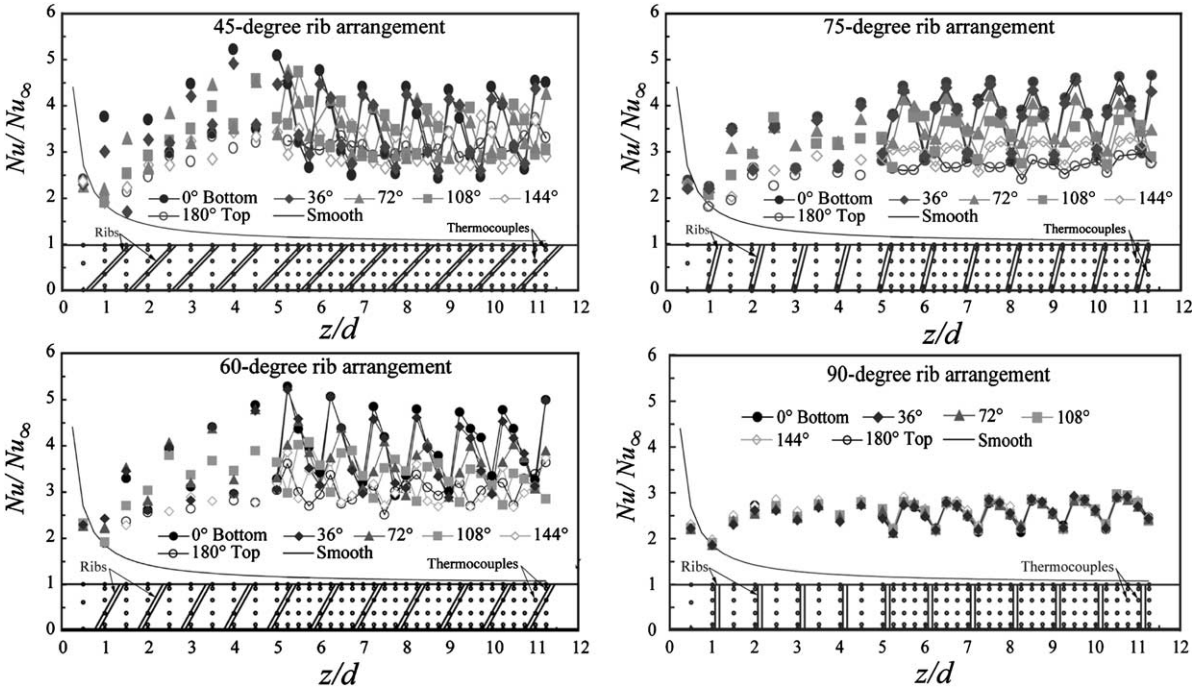


Fig. 4. *Nu* distribution inside a 90°, 75°, 60° and 45° rib-roughened circular tubes, $Re = 10,000$.

solved the governing equations sequentially. In this study pressure–velocity coupling algorithm SIMPLE was used. The calculations were made using the $k$–$\varepsilon$ model of turbulence.

The rib-roughened tube was generated in a way to be geometrically identical to that of the heat transfer test section.The Tet/Hybrid scheme was used in order to generate a very dense grid from preliminary tetrahedral elements with overall two million fine cells. Some hexahedral, pyramidal, and wedge elements were used to facilitate the complicated tube structure. Calculations have been performed for the uniform velocity and temperature profile at the inlet to the test section. The value of Reynolds number based on the tube diameter ($d = 31$ mm) was $Re = 15,000$. The turbulence intensity at the inlet was calculated as follows:

$$(I = u'/u_{\mathrm{m}} = 0.16(Re)^{-1/8}) \tag{8}$$

The outflow boundary condition was set to a free outflow. A fixed heat flux was generated on the tube surface (827 W/m$^2$) with the wall thickness of 1 mm.

## 3. Results and discussion

### 3.1. Heat transfer results

The measured Nusselt number distributions along each of the six lines of measurement points (thermocouples), representing half of the test section, for the cases of 90°, 75°, 60° and 45° rib-roughened tubes are presented in Fig. 4. (The circumferential location of the six lines of measurement points is illustrated in Fig. 5) It is shown in this figure that at first the *Nu*, in the case of 90° ribs, decreases at the inlet region of the test section as a result of the thermal boundary layer growth, then it increases. At around $z/d = 3$ it stabilizes in a repeated up-and-down fluctuation mode corresponding to the rib location. This mechanism of *Nu* enhancement by the 90° ribs in comparison to the Smooth surface (solid line) is based on the two-dimensional flow phenomena, flow separation and reattachment induced by these ribs. From the reattachment point the *Nu* enhancement rapidly deteriorates due to the boundary layer growth and the flow separation in front of the next rib. (This two-dimensional flow phenomenon has been already described by many researchers in the past; therefore, it does not need a closer examination.)

In contrast to the transverse ribs, the oblique ribs (75°, 60° and 45° ribs, respectively) show a strong *Nu* augmentation after the initial boundary layer growth at the inlet of the test section. It can be clearly observed in these graphs that the *Nu* distribution for the entire tube is higher for the oblique ribs than for the transverse ribs. Furthermore, the circumferential distribution of the *Nu* is not uniform, with the highest *Nu* occurring at the tube Bottom region (compare Bottom (•) and Top (○)). In the cases of the 60° and 45° ribs, the *Nu* achieves its

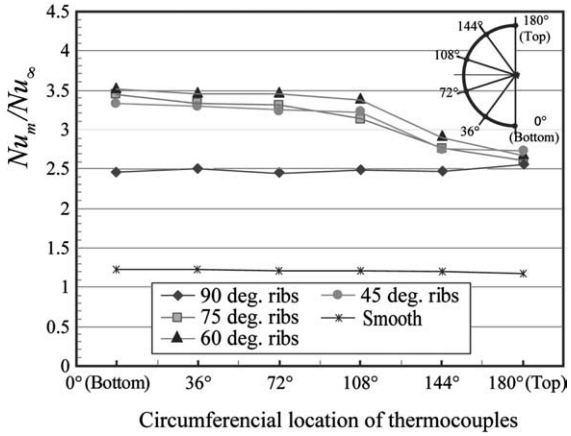


Fig. 5. Mean circumferential $Nu_m$ distribution along the lines of measurement points in the range of $z/d = 1$–11.

maximum at around $z/d = 4$–5, then the $Nu$ slightly decreases until it stabilizes at a certain level. In comparison to the former two cases, the $Nu$ distribution for the 75° ribs is rather more uniform and the $Nu$ augments continuously throughout the whole test section.

The heat transfer superiority of angled ribs over the conventional transverse ribs can be also confirmed in Fig. 5, by a significant $Nu_m$ augmentation ($Nu_m$—mean Nusselt number distribution, along the lines of measurement points in the range of $z/d = 1$–11) at the Bottom regions in comparison to the Top regions of the rib-roughened tube with the highest $Nu_m$ achieved for the 60°.

### 3.2. Numerical simulation and flow visualization results

The development of velocity vector distribution inside the 45° rib-roughened circular tube obtained by the

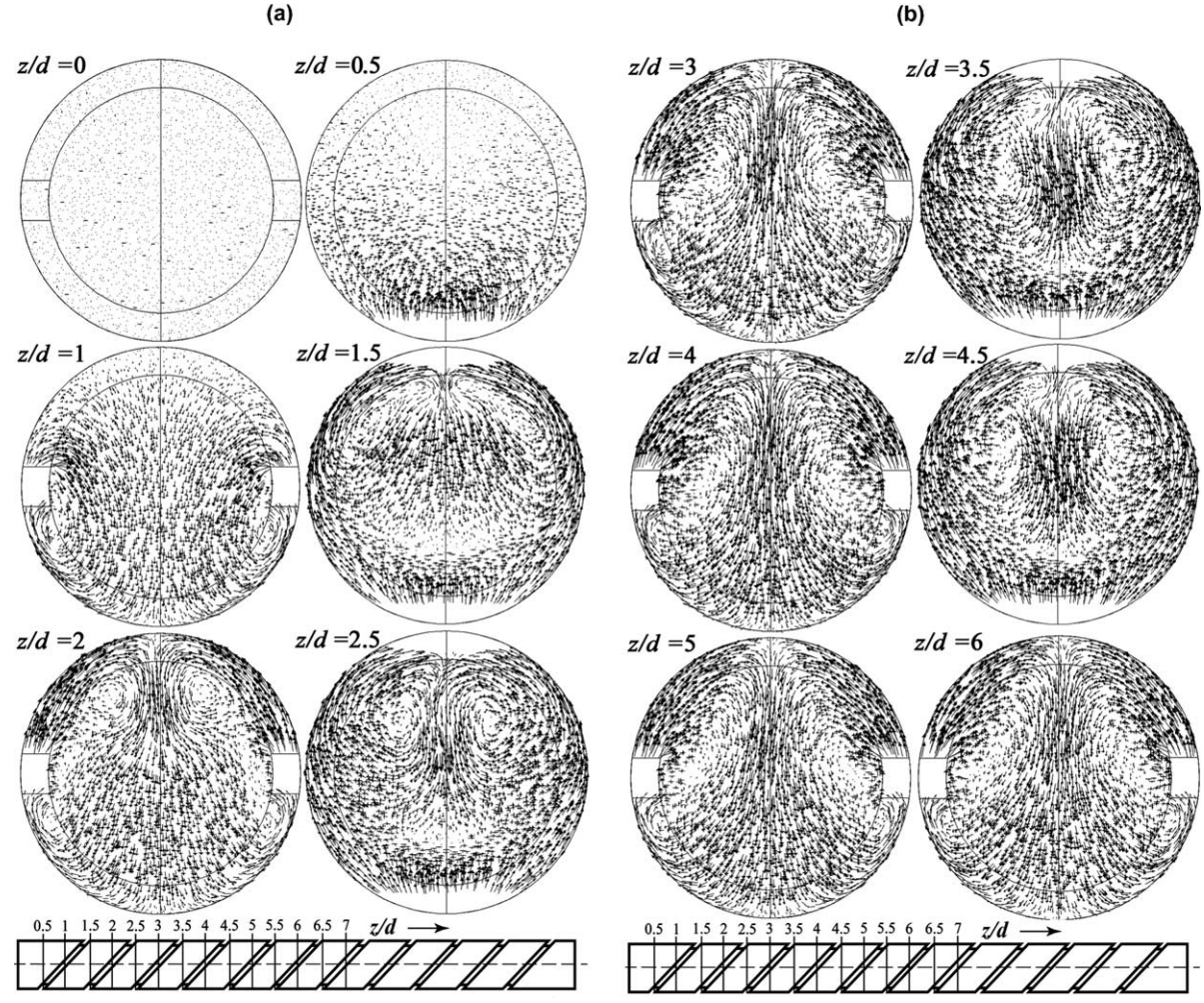


Fig. 6. (a) Development of the rib-induced secondary flow for the 45° ribs from $z/d = 0$–2.5, $Re = 15,000$. (b) Development of the rib-induced secondary flow for the 45° ribs from $z/d = 3$–6, $Re = 15,000$.

numerical simulation is presented in Fig. 6a and b. The flow at the entrance to the tube (at $z/d = 0$) is shown by a dotted field, which represents a uniform velocity profile or a given boundary condition, respectively. The flow proceeds into the tube and at $z/d = 0.5$ it encounters the first rib. At this point it moves in the direction of a minimum resistance, along the inclined rib walls as well as over the rib (white area with no vectors as the bottom part of the picture at $z/d = 0.5$). The flow near the tube surface, which initially moved along the inclined rib front wall, separates into two flow streams (from each side of the rib) and proceeds towards the tube Top region. Here these two streams encounter the "dead end" and they are forced to sharply turn and move towards the tube Bottom surface, as can be confirmed by a downward flow vectors in the central core region at $z/d = 1$ and $z/d = 1.5$. The presented flow structure strengthens with every additional rib and develops a secondary flow in a form of a pair of vortices, which convey the cold and higher-momentum fluid from the central core region towards the tube Bottom. This secondary flow reaches fully developed conditions at around $z/d = 4.5$–$5.0$.

A fundamentally similar flow behavior can be observed for the other two oblique rib arrangements. The 75° and 60° ribs also create the secondary flow in a form of a pair of vortices, as in the case of the 45° ribs, though with a weaker rotational velocity of the secondary flow, as can be seen in Fig. 7. The change of rib-inclination from $45° \rightarrow 60° \rightarrow 75°$ increases the distance needed for the fully developed secondary flow to be established:

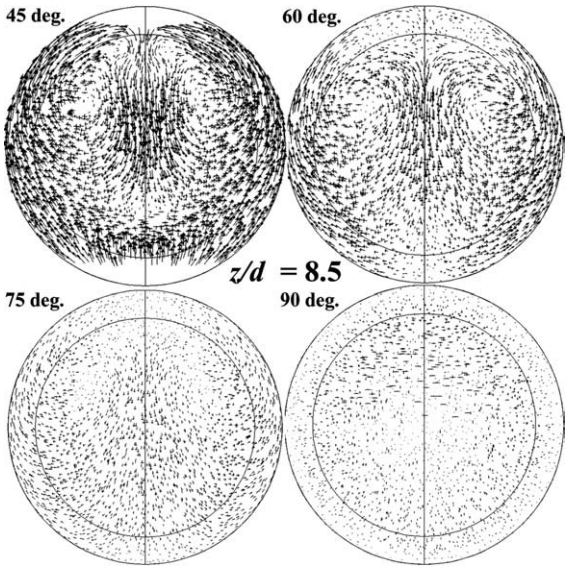


Fig. 7. Comparison among the secondary flow rotational momentums for all four rib patterns, $z/d = 8.5$, $Re = 15,000$.

$z/d = 4$–$5$ for the 45° ribs, at $z/d = 5$–$6$ for the 60° ribs and at $z/d = 6$ for the 75° ribs.

The strength of the secondary flow can be also confirmed in Fig. 8, which displays the side view velocity vector patterns obtained between $z/d = 6.5$–$9.5$ in the central vertical plane including the tube axis. It can be clearly observed here that the flow descent towards the tube bottom for the 45° ribs is the most severe. However with the change of rib-inclination ($45° \rightarrow 75° \rightarrow 60°$) it gradually diminishes until it completely disappears in the case of 90° ribs. One can also see a creation of separation bubbles just behind the ribs, in the Bottom region, and a flow reattachment taking place between two consecutive ribs.

The presented results obtained by numerical simulation closely coincided with the flow visualization results. Moreover, they provided us with a more detailed view on this complicated flow field (compare Figs. 8 with 9 or refer to [15,16]). All results (numerical simulation, heat transfer and flow visualization experiments) show a strong heat transfer superiority of the oblique ribs (75°, 60° and 45° ribs) over the transverse ribs. This fact is attributed to the development of the secondary flow, which diminishes the thickness of both velocity and thermal boundary layers and consequently augments the $Nu$. Besides, the $Nu_m$ of the tube Bottom surface shows considerably higher values in contrast to those on the tube Top surface, which can be credited to: (1) rotational direction of the secondary flow which conveys the cold fluid directly from the central core region to the heated surface and (2) strengthening of the flow reattachment between two consecutive ribs through the introduction of higher momentum fluid from the central core region of the tube. The highest $Nu_m$ at the Bottom regions was achieved for the 60° ribs due to the most optimal flow conditions generating considerably small separation regions just behind the ribs and at the same time inducing a strong secondary flow structure. It could be also concluded that the axial location of the initiation of fully developed secondary flow region agrees with the axial position where the $Nu$ maximum value in the cases the 60° and 45° ribs, as was mentioned previously.

### 3.3. Comparison with other studies

To the authors' knowledge, none of the published studies ever reported the concept of the rib-induced secondary flow in the form of a pair of vortices, which convey the colder fluid from the passage core region to the heated surface and appreciably increase the heat transfer performance on the part of the tube surface. However, it was confirmed by Liu and Jensen [14] and Gee and Webb [13] that the helically inclined ribs augment the heat transfer performance in comparison to the transverse ribs and that the highest heat transfer augmentation was obtained for the rib-inclination

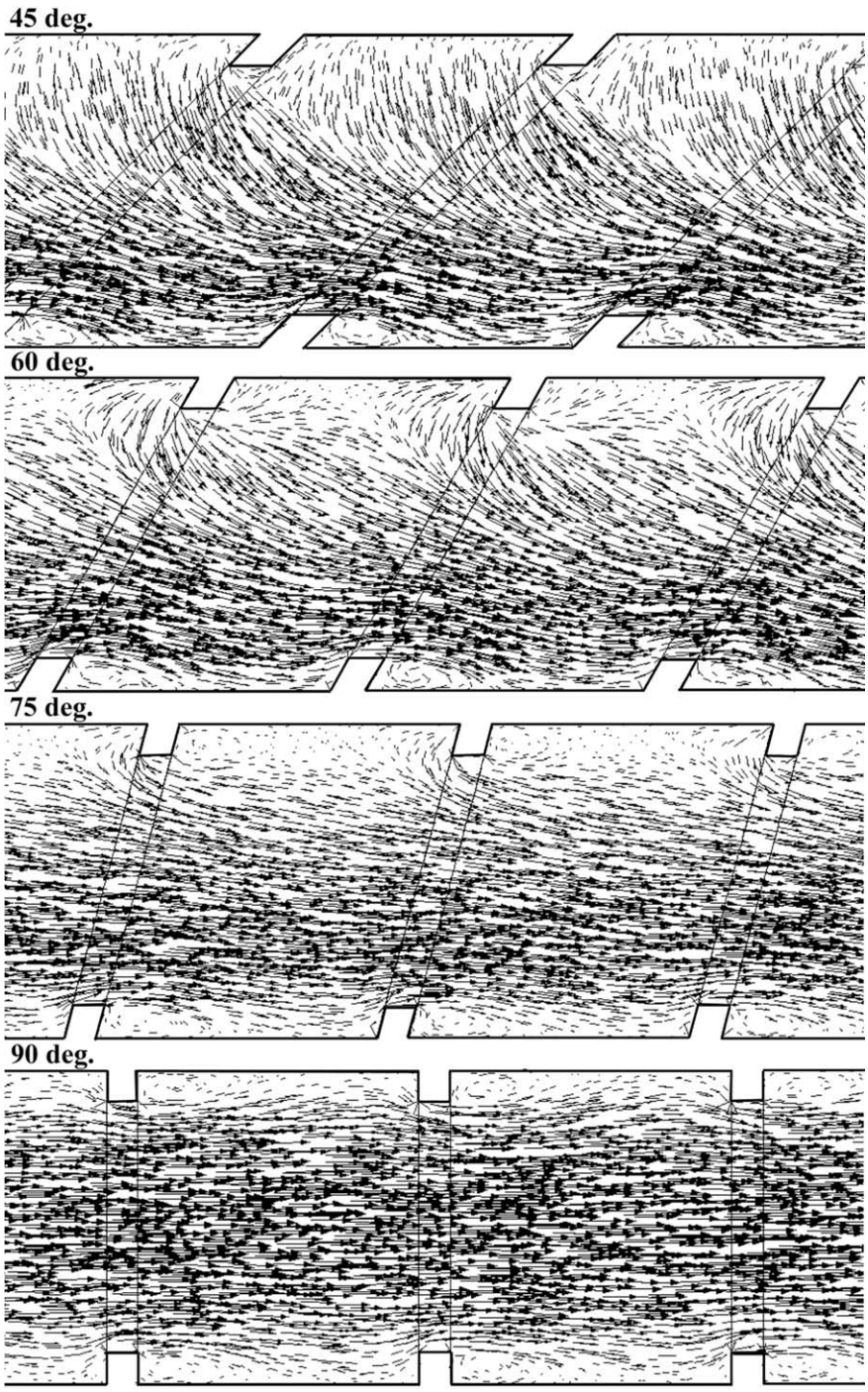


Fig. 8. Side view velocity vectors patterns obtained between $z/d = 6.5$–$9.5$ at the tube $z$-axis, $Re = 15,000$. Main flow direction from left to right.

somewhat around 60°. (The helically inclined ribs induce a secondary flow in the form of a single vortex, which is completely different flow behavior with the present study.)

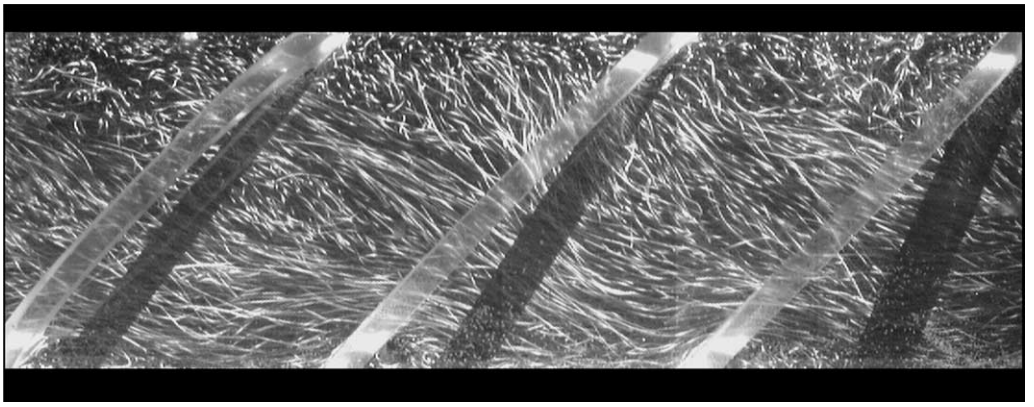

Fig. 9. Flow pattern obtained by the flow visualization for 45° ribs obtained between $z/d = 6.5$–9.5 at the tube $z$-axis, $Re = 15,000$. Main flow direction from left to right.

## 4. Conclusions

In the present study, detailed local heat transfer measurements and numerical simulation were conducted in order to understand the overall and detailed heat transfer distribution inside a rib-roughened tube. Two different types of ribs were employed: (a) angled ribs (elliptic rings) and (b) the transverse ribs (circular rings). They were mounted on the inner surface of a circular tube with the angle between the plane of each rib and the mean flow direction of 75°, 60° and 45° for the angled ribs and 90° for the transverse ribs. The following conclusions were drawn:

(1) The present study clearly demonstrated the heat transfer superiority of the angled ribs over the conventional transverse ribs. This is attributed to the development of the secondary flow in a form of a pair of vortices, which convey the colder fluid from the tube core regions towards the heated surfaces. Consequently, it augments the heat transfer by diminishing the thickness of both velocity and thermal boundary layers.
(2) In the case of angled ribs, the circumferential mean distribution of the Nusselt number, $Nu_m$, is the highest at the tube Bottom region as a result of the rotational direction of the secondary flow which conveys the cold fluid directly from the central core region towards the Bottom surface.
(3) The highest $Nu_m$ at the Bottom regions was achieved for the 60° ribs due to the most optimal flow conditions generating considerably small separation regions just behind the ribs and at the same time inducing a strong secondary flow structure.
(4) The change in the rib-inclination ($45° \rightarrow 60° \rightarrow 75° \rightarrow 90°$) results in: (a) deterioration of the rotational momentum of the rib-induced secondary flow and (b) increase of the distance needed to achieve the fully developed secondary flow field.

## References

[1] R.L. Webb, Principles of Enhanced Heat Transfer, John Wiley & Sons, Inc., Professional, Reference and Trade Group, New York, NY, 1994, 10158-0012.
[2] S. Nozu, H. Honda, Condensation of refrigerants in horizontal, spirally grooved microfin tubes: numerical analysis of heat transfer in the annular flow regime, J. Heat Transfer 122 (2000) 80–91.
[3] I. Alam, P.S. Ghoshdastidar, A study of heat transfer effectiveness of circular tubes with internal longitudinal fins having tapered lateral profiles, Int. J. Heat Mass Transfer 45 (2002) 1371–1376.
[4] L.J. Brognaux, R.L. Webb, L.M. Chamra, B.Y. Chung, Single phase heat transfer in micro-fin tubes, Int. J. Heat Mass Transfer 40 (18) (1997) 4345–4357.
[5] W.J. Marner, A.E. Bergles, J.M. Chenoweth, On the presentation of performance data for enhanced tubes used in shell-and-tube heat exchanger, J. Heat Transfer 105 (1983) 358–365.
[6] R. Sethumadhavan, M.R. Raja, Turbulent flow friction and heat transfer characteristics of single and multistart spirally enhanced tubes, J. Heat Transfer 108 (1986) 55–61.
[7] X.D. Chen, X.Y. Xu, S.K. Nguang, A.E. Bergles, Characterization of the effect of corrugation angles on hydrodynamic and heat transfer performance of four-start spiral tuber, J. Heat Transfer 123 (2001) 1149–1158.
[8] G.J. Kidd, The heat transfer and pressure-drop characteristics of gas flow inside spirally corrugated tubes, J. Heat Transfer (August) (1970) 513–519.
[9] N.L. Vulchanov, V.D. Zimparov, L.B. Delov, Heat transfer and friction characteristics of spirally corrugated tubes for power plant condensers-2. A mixing-length model for predicting fluid friction and heat transfer, Int. J. Heat Mass Transfer 34 (9) (1991) 2199–2206.
[10] V.D. Zimparov, V.D. Vulchanov, L.B. Delov, Heat transfer and friction characteristics of spirally corrugated

tubes for power plant condensers—experimental investigation and performance evaluation, Int. J. of Heat Mass Transfer 34 (9) (1991) 2187–2197.

[11] R.L. Webb, E.R.G. Eckert, R.J. Goldstein, Generalized heat transfer and friction correlations for tubes with repeated rib roughness, Inter. J. Heat and Mass Transfer 15 (1972) 180–184.

[12] R.L. Webb, E.R.G. Eckert, Application of rough surfaces to heat exchanger design, Int. J. Heat Mass Transfer 15 (1972) 1647–1658.

[13] D.L. Gee, R.L. Webb, Forced convection heat transfer in helically rib-roughened tubes, Int. J. Heat Mass Transfer 23 (1980) 1127–1136.

[14] X. Liu, M.K. Jensen, Geometry effects on turbulent flow and heat transfer in internally finned tubes, J. Heat Transfer 123 (2001) 1035–1044.

[15] R. Kiml, S. Mochizuki, A. Murata, Heat transfer augmentation by rib-induced secondary flow inside a circular tube, Proceedings of 13th International Symposium on Transport Phenomena, Victoria, Canada, 2002, (15–18 July 2002), pp. 291–295.

[16] S. Mochizuki, R. Kiml, A. Murata, V. Stoica, Heat transfer enhancement by rib-induced secondary flow inside a circular tube, CD-ROM Proceedings of 12th International Heat Transfer Conference, Grenoble, France, August 18–23th 2002, vol. 4, pp. 141–146.

[17] R. Kiml, S. Mochizuki, A. Murata, V. Stoica, Effects of rib-induced secondary flow on heat transfer augmentation inside a circular tube, J. Enhanc. Heat Transfer 10 (1) (2003) 9–20.